DOR: 20.1001.1.27170314.2022.11.4.5.7

Research Paper

Impact of FSP Tool Probe Shape on Reinforcing Particles Dispersion in the Piston Alloy Using CEL Approach

Mostafa Akbari[1*], Hossein Rahimi Asiabaraki[1], Ezatollah Hassanzadeh[1]
[1]Department of Mechanical Engineering, Technical and Vocational University (TVU), Tehran, Iran
[*]Email of the Corresponding Author: mo-akbari@tvu.ac.ir, mr.mostafaakbari@yahoo.com
Received: November 24, 2022; Accepted: January 14, 2023

Abstract
In this study, the distribution of boron carbide in the stir zone of the FSPed specimens was examined experimentally and numerically about probe shape, including circular, square, and hexagonal shapes. First, composites were created using different tools. Then, using an optical microscope, the microstructural properties of the samples, such as the size and shape of the silicon particles, were examined. To simulate the procedure and further explore particle distribution, the coupled Eulerian-Lagrangian (CEL) method is employed. The tool was also modeled using a Lagrangian formulation while the material was characterized using an Eulerian formulation. The model predicted the changes in strain and temperature in composites created with different probe shapes. The outcome demonstrated that the circular probe was not suitable for the production of composites because it could not disperse particles in the parent alloy. Tools with flat surfaces, such as square and hexagonal tools, have more evenly distributed metal particles. Square probes can be employed in the FSP process to create composites and offer the best performance in terms of reinforcing particle distribution in the metal matrix. Due to the greater distribution of reinforcing particles, the sample made with a square tool had the highest hardness. Using a tool with a square pin improves the average hardness by 8 and 21%, respectively, compared to hexagonal and circular tools.

Keywords
Composite, CEL Method, Particle Distribution, Microstructural, Hardness

1. Introduction

Aluminum and its alloys are extensively used in the construction of ships, airplanes, and other forms of transportation due to its distinctive attractiveness in manufacturing lightweight objects. However, many technical applications, especially those requiring surface contact, do not suit these metals [1, 2]. Their use has therefore been constrained. Researchers have used various methods to improve the performance of these alloys to achieve that goal [3, 4].

The FSP method is one of the widely used methods to modify the microstructural properties of metals and also to produce metal-based composites [5, 6]. This method is similar to the friction stir welding method, with the difference that metal joining is not required. Furthermore, these methods use identical parameters and equipment. In this method, a rotating tool with a particular geometry that

has a comb and a pin enters the sample and creates microstructural changes [7]. Also, in this method, metal composites can be created by embedding reinforcing particles in the alloy.

The homogenous dispersion of reinforcement particles in the parent metal is one of the main issues in the manufacture of metal-based composites [8, 9]. In conventional methods of composite production, the accumulation of reinforcement particles in the parent alloy is abundant. This accumulation of reinforcement particles severely diminishes the mechanical characteristics of the resulting composite. One technique that can disperse the reinforcing particles in the parent metal more effectively is the FSP approach. However, the design of the FSP tool probe ultimately determines how well this procedure works. Al-CNT composites were created by Sharma et al. [10] using the FSP technique. They applied a tool with a circular probe to spread the particles in the aluminum matrix. Their findings showed that the generated composite's particle accumulation was improperly dispersed. Darzi Bourkhani et al. [11] investigated the effect of probe diameter on the tensile properties of nanocomposites. To create composite specimens, they used cylinder tools with diameters of 4, 6, and 8 mm. They discovered that if Al_2O_3 particles aggregated to form coarse particles, ductility would suffer. The sample made with instruments that had an 8 mm diameter had the maximum particle accumulation. In this sample, extremely coarse agglomerated particles formed, erasing the beneficial effects of grain refinement on ductility and leading to noticeably poorer composite ductility. Using friction stir processing (FSP), Li et al. [12] fabricated AA6061/316 surface composites using single and double-pin tools. According to their findings, a significant difference in reinforcement particle dispersion was observed when the number of pins was increased from 1 pin to 2 pins. The effect of hybrid pin profiles on AA5052/SiC surface composites fabricated via friction stir processing was investigated by Sarvaiya et al. [13]. Based on the results, it was determined that the hybrid pin tool distributed SiC particles uniformly due to lateral downward movement and pulsation.

It's essential to achieve some process elements, including temperature and strain distribution, to comprehend the process better [14-16]. Using experimental techniques to study these factors is exceedingly challenging and frequently impossible. Numerical techniques have been created specifically to examine these phenomena [17, 18]. Recently, the CEL method was used to simulate severe plastic deformation (SPD) [19-21]. The material domain is specified using an Eulerian formulation, which may prevent significant mesh distortion. Al-Badour et al. [22] used the CEL technique to predict volumetric flaws like tunnels during the FSW of aluminum. The CEL approach was employed by Akbari et al. [15, 23] to look at the materials mixing in the SZ during the FSW process. To investigate commonly occurring defects in FSW processes, Das et al. [24] developed a coupled Eulerian–Lagrangian (CEL) finite element model. Ragab et al. [25] developed a finite element model based on the Coupled Eulerian Lagrangian (CEL) approach to investigate the FSW of steel. They stated that a higher tool rotation rate resulted in a higher peak temperature, greater plastic strain, rougher surface, and larger flash size.

As seen, the experimental investigation of the tool pin effect in the FSP process has been investigated by previous researchers, although experimental methods cannot study many process parameters. For this purpose, in this research, the effect of the tool pin on the distribution of reinforcing particles is studied by simultaneously using experimental and numerical methods, which is one of the innovations of this research. Various probe shapes used in earlier research were gathered and examined to discover

the best tool probe for composite manufacture with suitable particle dispersion. After creating the composites using various probes, macro photos were used to examine how the particles were distributed within the parent alloy. Information on temperature variations and strain generated by each probe during the operation is required to determine the causes of altering the dispersing pattern of particles in the parent alloy using different probes. The CEL approach was used to gather this data using process modeling.

2. Experimental method

A356 alloy, with chemical compositions listed in Table 1, was used to fabricate composites.

Table 1. Chemical composition of A356 aluminum alloy

Element	wt (%)
Si	7
Fe	0.31
Cu	0.2
Mn	0.1
Mg	0.3
Zn	0.1
Ti	0.25

In this experiment, B_4C reinforcement with an average size of 10 m was used from commercial sources. B_4C particles were inserted for composite manufacturing into a groove that had dimensions of 1.4 mm in width and 3.5 mm in depth. To prevent reinforcement particles from escaping during FSP, the tool, without a probe, initially sealed the grooves' surface. The plate was next treated by FSP using a tool with a varied probe shape for four passes down the groove.

Hardened H13 tools with various tool probe shapes, including circular, square, and hexagonal, were used in this study to examine the impact of the tool probe shape on particle dispersion in the metal matrix. Dimensions of the FSP instruments used in this work are shown in Figure 1. The FSP tool tilt angle was held constant across all trials at 3°. The tool traverse and rotational speeds were maintained throughout all experiments at 1200 RPM and 32 mm/min, respectively.

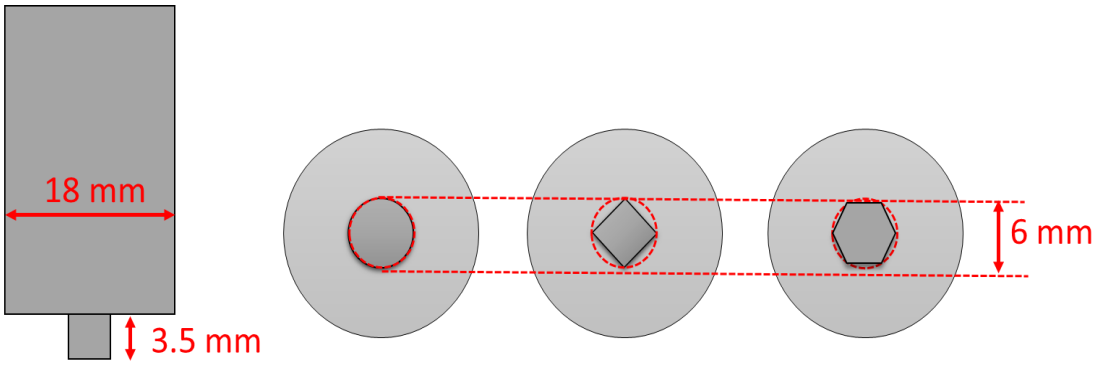

Figure 1. Specifications of the tools used in the process

After FSP, the composites' microstructure was examined using a metallurgical microscope. According to normal metallographic methods, the FSPed specimens were mechanically polished and etched with Keller's reagent. The composites' microhardness at various places in the stir zone was assessed with a 200 g load applied, and a 15 s dwell time (SZ).

3. Model description

To predict temperature and strain during composite manufacture using the FSP approach, a three-dimensional CEL methodology is applied. Eulerian analysis, in which the nodes are fixed, and the material travels across the fixed meshes, can correct mesh distortion in FSP modeling. As a result, the workpiece was specified as an Eulerian body with EC3D8RT components, and the tool was defined as a rigid isothermal Lagrangian body. The CEL model models aluminum as the parent metal and does not consider reinforcement particles. The complete set of governing modeling equations for the CEL approach can be found in the authors' earlier work.[15, 23]. Temperature, strain, and strain rate all affect the flow stress in FSP.

Convective heat transfer coefficients vary depending on the surface. To save time, the backing plate is disregarded, and a convective heat transfer coefficient of 6000 W/m^2.°C is established at the bottom. The equivalent value at the top surface of the samples was set to 50 W/(m^2.°C) to account for heat loss through natural convection. All motion requirements are specified regarding the tool's reference point to control FSP tool movement correctly (Figure 2).

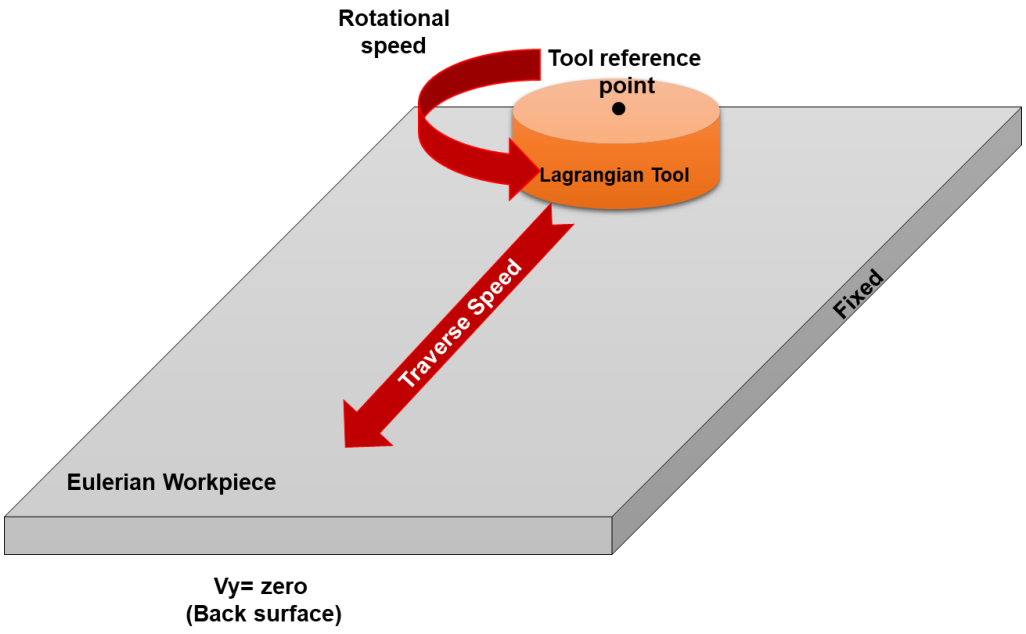

Figure 2. Boundary conditions used in the model

Besides the contact between the FSP tool and the workpiece, the stirring action causes self-contact inside the materials in the SZ. All tool and material interactions were referred to as general contact interactions. To simulate friction between tools and workpieces, Coulomb's law of friction was applied.

For the described model, a mesh size of 1.2 mm (Figure 3) is almost perfect. The tool is modeled as an isothermal Lagrangian rigid body by the 4-node 3D bilinear rigid quadrilateral components. Additionally, the tools mesh with 0.7 mm elements.

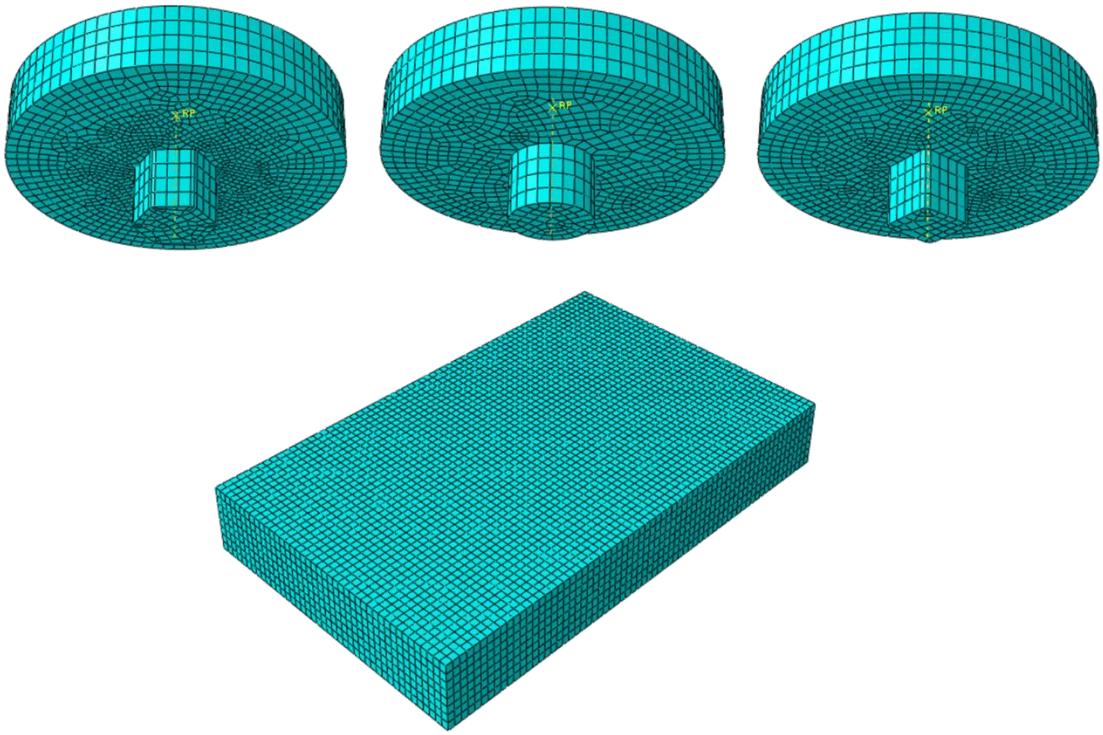

Figure 3. Meshed tools and workpieces in the numerical model

4. Result and discussion

4.1 Particle distribution and microstructure in composites

The microstructures of the A356 parent alloy are shown in Figure 4. As seen in this image, there were coarse acicular silicon particles, and the Si particles' dispersion within the metal matrix was not uniform. This microstructure contributes to the alloy's brittle nature.

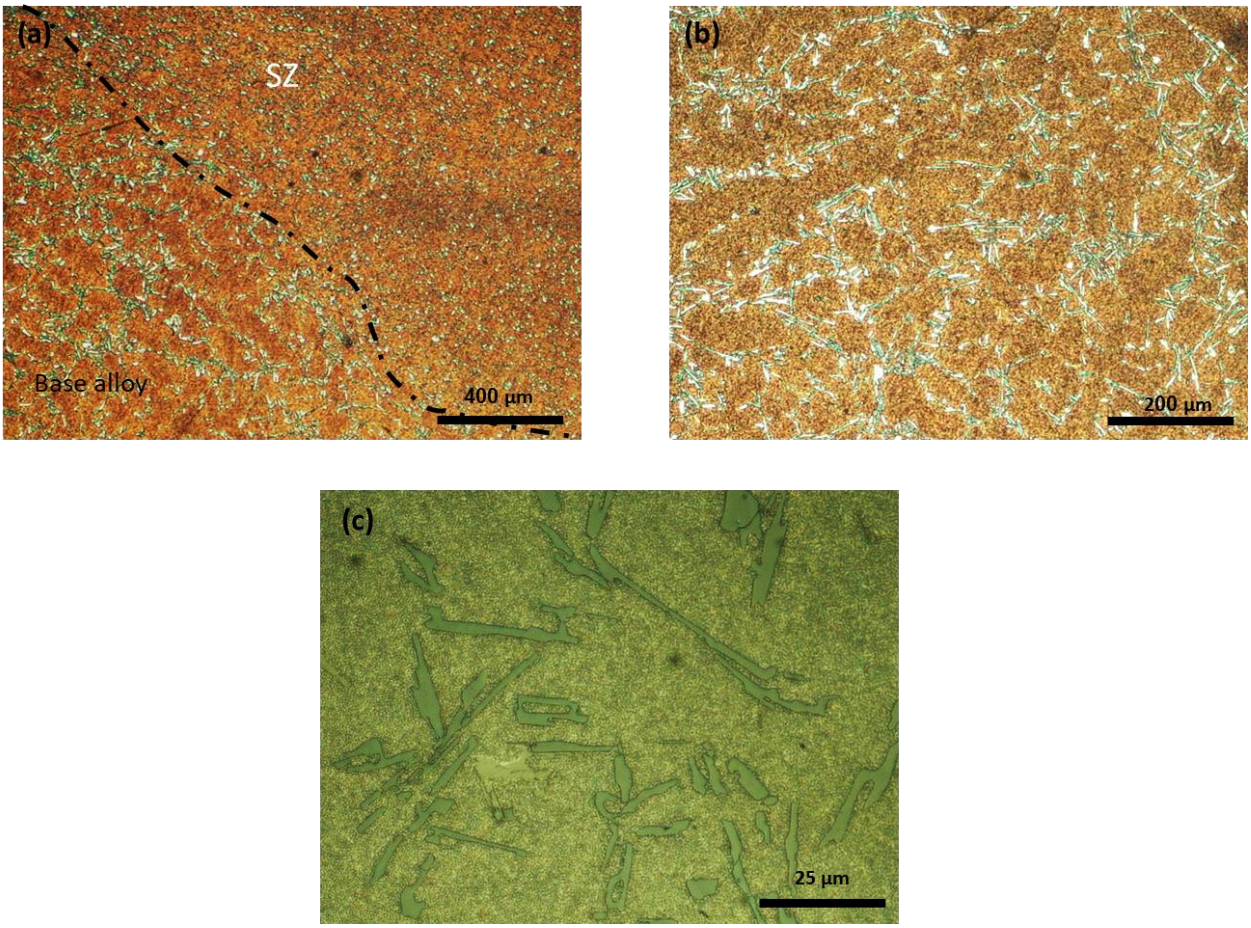

Figure 4. Microstructural images of a) different areas of the FSPed sample, b and c) base metal

Figure 5 illustrates the microstructure of the SZ of the FSPed specimens without reinforcing particles. Silicon particles were dispersed evenly throughout the SZ after breaking up into coarse needle-like particles. Additionally, the dendritic microstructure of the parent alloy was destroyed. Si particles of the coarse needle type are divided into tiny pieces. This results from temperature exposure and severe plastic deformation that occurred during FSP. Additionally, FS-Processed A356 has no porosity, which is consistent with earlier observations [26, 27]. Also, compared to the circular tool, the square tool has turned the needle-shaped Si particles into smaller particles.

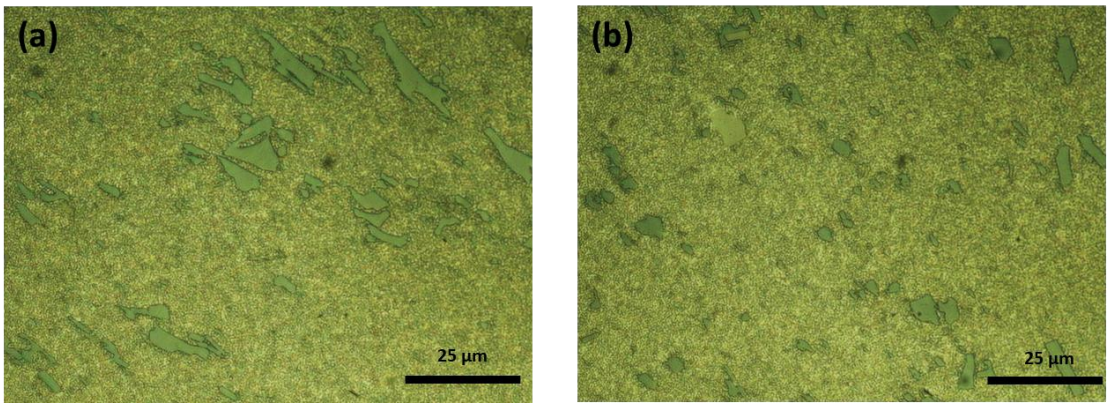

Figure 5. Microstructural photos of composites produced with a) circular tool b) square tool

Figure 6 displays macro pictures of the FSPed samples made with several probe profiles, including cylinder, square, and hexagonal. The FSP specimens appear to be flawless, while the SZ has a basin-like shape. Particles were not evenly dispersed throughout the samples made using the circular probe profile, as seen in Figure 6. When a circular probe profile is utilized, the creation of various transverse bands with various particle percentages may be because of insufficient material strain. It can be inferred that the probe profile with a flat surface has a stronger eccentricity and pulsation effect, which increases material flow while improving particle distribution compared with the circular probe profile. The probe cross-section for the circular probe profile is the same in both static and dynamic drawings since there is no pulsation effect. But there is a distinction between static and dynamic illustrations of the hexagonal and square probe profiles [28]. Although the hexagonal probe produces approximately 50% more pulses than the square probe, the square probe's revolving arm is larger. Figure 6 illustrates how using the square probe tool rather than the hexagonal tool results in a better distribution of the reinforcement particles. Strain and temperature are computed during the process using numerical simulation to investigate the cause of the square tool's superiority. Figure 6 displays the strain distribution at the composite cross-section created using various probes throughout the process. Compared to other probes, it turns out that the circular tool's strain has the lowest value. This low strain is consistent with the experimental findings of the manufactured composite and points to an insufficient material flow during the process that prevents the reinforcing particles from dispersing properly in the aluminum phase. The strain is much greater than with circular tools in samples made with tools with flat surfaces. The tool with the square probe, as seen, causes the most strain in the sample. When using tools with smooth surfaces, the strain is increased and the revolving arm and pulsation effect primarily improve the material flow. Increasing the number of edges reduces the peak strain while simultaneously increasing the area subject to the strain. The square tool is under the most stress because it has the largest rotating arm compared to other probes.

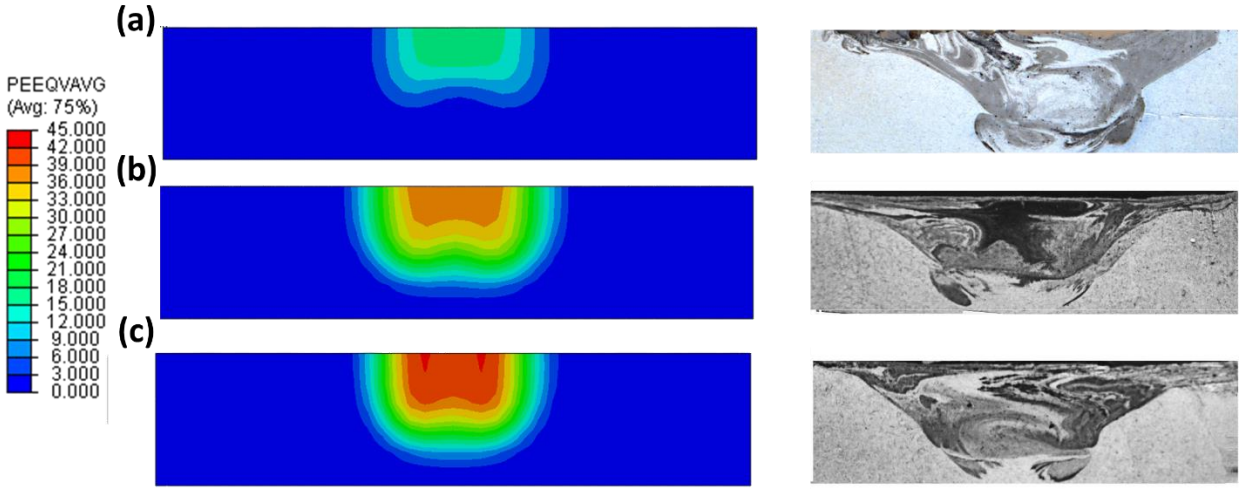

Figure 6. Macro image of the SZ and the strain created in the samples produced with a) circular tool, b) hexagonal tool c) square tool

The temperature distribution at the cross-section of the composite using various probes is shown in Figure 7. It turns out that all of the samples' temperature changes are only marginally different from one another. The minimal temperature variation between the various samples is caused by the fact that the tool shoulder, which generates most of the heat produced throughout the procedure, is the same size for all tools. According to these findings, there isn't much of a difference between the temperature histories of samples made with various equipment; therefore, the temperature cannot account for changes in the particle dispersion pattern when using various probes.

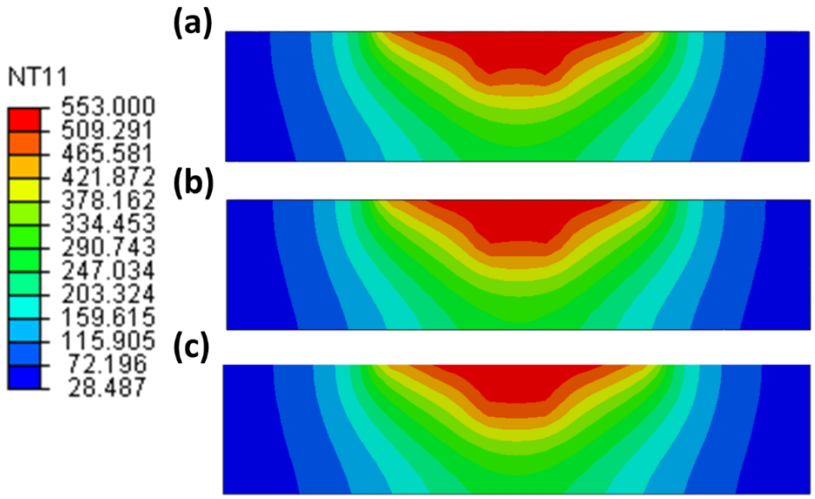

Figure 7. Temperature changes in samples produced with a) circular tool, b) hexagonal tool c) square tool

4.2 Hardness

The microhardness profile of the B_4C composite layer created by various tool probe profiles is shown in Figure 8. The hardness of the composites is noticeably higher than that of the parent alloy, as seen in this figure. There are several causes for this growth. First, the microstructural improvements made during FSP, such as the breaking up of Si particles, the removal of coarse α-Al dendrites, and grain

refining, increase the hardness of the SZ. As a result of the Si needles being broken down and homogenized, Shinoda and Kawai [29] concluded that the SZ becomes harder.

Second, the presence of reinforcement particles with very high hardness at the stir zone of the piston alloy matrix improves hardness. Additionally, the A356 parent alloy and the B_4C reinforcing particles have very different coefficients of thermal expansion, which causes more geometrically required dislocations (GNDs) to form during heat cycles [30, 31]. Another factor contributing to improved hardness is the Orowan strengthening mechanism. The latter mechanism, however, improves hardness less effectively for reinforcements made of micron-sized particles and works better when particle size is decreased.

Another noteworthy finding is the variance in microhardness values for composites made using square, circular, and hexagonal probe shapes. This finding may be connected to the non-uniform homogeneous distribution of B_4C in the metal matrix. Less variation in the microhardness profiles occurs when the reinforcing particles are distributed uniformly. The composite generated by square probes exhibits an average microhardness of 82.61 HV (Figure 8).

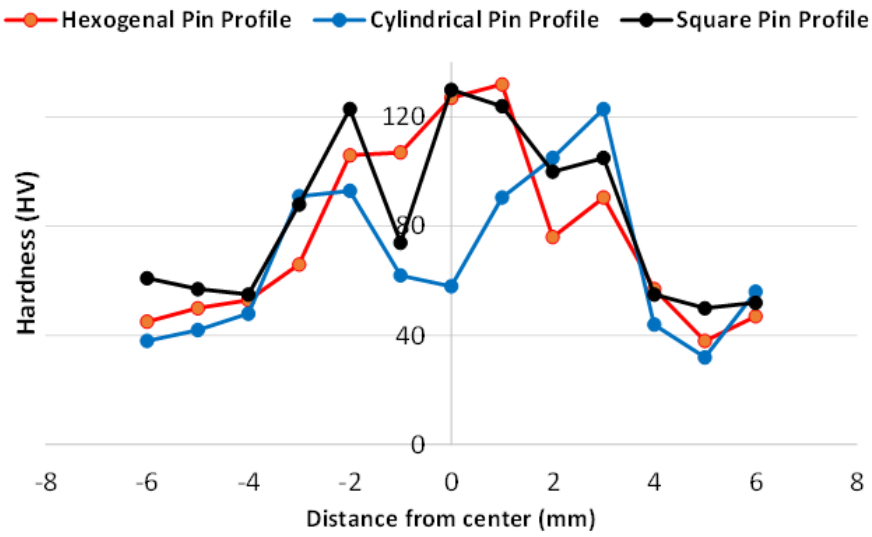

Figure 8. Hardness changes in the cross-section of samples produced with different tools

5. Conclusion

This study investigates the impact of the probe profile on the dispersion of reinforcing particles within the metal matrix. The coupled Eulerian-Lagrangian (CEL) method is used to analyze particle dispersion further and explain the process. The workpiece is modeled using an Eulerian formulation, whereas the tool is described using a Lagrangian formulation. In conclusion, this study's findings were as follows.

- After the FSP process, the needle-shaped silicon particles were transformed into small circular particles. Also, the square tool produced smaller particles than the circular tool because of having smooth surfaces and thus creating more strain.
- The results showed that the circular probe could not evenly distribute the particles.
- Comparing samples created with square probes to samples created with circular tools, the particle dispersion in the samples created by the square probes is significantly better.

- The maximum strain depends on the revolving arm's value.
- The fundamental element in particle dispersal in the metal matrix is the pulsing effect of the probe.
- The maximum hardness was obtained in the sample produced with a square tool because of the better distribution of reinforcing particles.

6. References

[1] Yadegari, H., Taherian, R. and Dariushi, S. 2021. Investigation on mechanical properties of hybrid aluminum/composite tubes manufactured by filament winding and hand lay-up. Polymers and Polymer Composites. 29(9_suppl): S1486-S1497.

[2] Rajendran, C., Srinivasan, K., Balasubramanian, V., Balaji, H. and Selvaraj, P. 2021. Feasibility study of fsw, lbw and tig joining process to fabricate light combat aircraft structure. International Journal of Lightweight Materials and Manufacture. 4(4): 480-490.

[3] Fathi, J., Ebrahimzadeh, P., Farasati, R. and Teimouri, R. 2019. Friction stir welding of aluminum 6061-t6 in presence of watercooling: Analyzing mechanical properties and residual stress distribution. International Journal of Lightweight Materials and Manufacture. 2(2): 107-115.

[4] Akbari, M., Asadi, P. and Rahimi Asiabaraki, H. 2021. Improving the hardness and microstructural properties of piston alloy using the fsp method. Journal of Modern Processes in Manufacturing and Production. 10(2): 53-62.

[5] Zolghadr, P., Akbari, M. and Asadi, P. 2019. Formation of thermo-mechanically affected zone in friction stir welding. Materials Research Express. 6(8): 086558.

[6] Afsari, A., Heidari, S. and Jafari, J. 2020. Evaluation of optimal conditions, microstructure, and mechanical properties of aluminum to copper joints welded by fsw. Journal of Modern Processes in Manufacturing and Production. 9(4): 61-81.

[7] Rezaee Hajideh, M., Farahani, M. and Khanbeigi, M.A. 2017. A hybrid thermal assisted friction stir welding approach for pmma sheets. Journal of Modern Processes in Manufacturing and Production. 6(2): 51-60.

[8] Shojaeefard, M.H., Akbari, M., Asadi, P. and Khalkhali, A. 2016. The effect of reinforcement type on the microstructure, mechanical properties, and wear resistance of a356 matrix composites produced by fsp. The International Journal of Advanced Manufacturing Technology.): 1-17.

[9] Akbari, M., Asadi, P., Besharati Givi, M.K. and Khodabandehlouie, G. 2014. Artificial neural network and optimization, in Advances in Friction-Stir Welding and Processing, Woodhead Publishing, Elsevier.

[10] Sharma, A., Fujii, H. and Paul, J. 2020. Influence of reinforcement incorporation approach on mechanical and tribological properties of aa6061- cnt nanocomposite fabricated via fsp. Journal of Manufacturing Processes. 59: 604-620.

[11] Darzi Bourkhani, R., Eivani, A.R., Nateghi, H.R. and Jafarian, H.R. 2020. Effects of pin diameter and number of cycles on microstructure and tensile properties of friction stir fabricated aa1050-al2o3 nanocomposite. Journal of Materials Research and Technology. 9(3): 4506-4517.

[12] Li, S., Paidar, M., Liu, S., Mehrez, S., Kumar, P.S. and Mohanavel, V. 2022. Importance of pin number on mechanical properties and wear performance during manufacturing of aa6061/316 surface composite via fsp. Materials Letters. 326: 132919.

[13] Sarvaiya, J. and Singh, D. 2022. Influence of hybrid pin profile on enhancing microstructure and mechanical properties of aa5052/sic surface composites fabricated via friction stir processing. The Canadian Journal of Metallurgy and Materials Science. 1-14: https://doi.org/10.1080/00084433.2022.2114124.

[14] Asadi, P., Akbari, M. and Karimi-Nemch, H. 2014. Simulation of friction stir welding and processing, Advances in Friction-Stir Welding and Processing. Woodhead Publishing, Elsevier.

[15] Akbari, M., Asadi, P. and Behnagh, R.A. 2021. Modeling of material flow in dissimilar friction stir lap welding of aluminum and brass using coupled eulerian and lagrangian method. The International Journal of Advanced Manufacturing Technology. 113(3): 721-734.

[16] Mohammadi Kuhbanani, H., Yasemi, H. and Aghajani Derazkola, H. 2018. Effects of tool tilt angle and plunge depth on properties of polycarbonate fsw joint. Journal of Modern Processes in Manufacturing and Production. 7(4): 41-55.

[17] Asadi, P., Mirzaei, M. and Akbari, M. 2022. Modeling of pin shape effects in bobbin tool fsw. International Journal of Lightweight Materials and Manufacture. 5(2): 162-177.

[18] Akbari, M. and Asadi, P. 2021. Simulation and experimental investigation of multi-walled carbon nanotubes/aluminum composite fabrication using friction stir processing. Proceedings of the Institution of Mechanical Engineers, Part E: Journal of Process Mechanical Engineering. 235(6): 2165-2179.

[19] Grujicic, M., Snipes, J.S., Ramaswami, S., Galgalikar, R., Yen, C.F. and Cheeseman, B.A. 2017. Computational analysis of the intermetallic formation during the dissimilar metal aluminum-to-steel friction stir welding process. Proceedings of the Institution of Mechanical Engineers, Part L: Journal of Materials: Design and Applications. 233(6): 1080-1100.

[20] Chu, Q., Yang, X.W., Li, W.Y., Vairis, A. and Wang, W.B. 2018. Numerical analysis of material flow in the probeless friction stir spot welding based on coupled eulerian-lagrangian approach. Journal of Manufacturing Processes. 36: 181-187.

[21] Akbari, M. and Asadi, P. 2021. Optimization of microstructural and mechanical properties of brass wire produced by friction stir extrusion using taguchi method. Proceedings of the Institution of Mechanical Engineers, Part L: Journal of Materials: Design and Applications. 235(12): 2709-2719.

[22] Al-Badour, F., Merah, N., Shuaib, A. and Bazoune, A. 2013. Coupled eulerian lagrangian finite element modeling of friction stir welding processes. Journal of Materials Processing Technology. 213(8): 1433-1439.

[23] Akbari, M. and Asadi, P. 2020. Dissimilar friction stir lap welding of aluminum to brass: Modeling of material mixing using coupled eulerian–lagrangian method with experimental verifications. Proceedings of the Institution of Mechanical Engineers, Part L: Journal of Materials: Design and Applications. 234(8): 1117-1128.

[24] Das, D., Bag, S. and Pal, S. 2021. A finite element model for surface and volumetric defects in the fsw process using a coupled eulerian–lagrangian approach. Science and Technology of Welding and Joining. 26(5): 412-419.

[25] Ragab, M., Liu, H., Yang, G. J. and Ahmed, M.M.Z. 2021. Friction stir welding of 1cr11ni2w2mov martensitic stainless steel: Numerical simulation based on coupled eulerian lagrangian approach supported with experimental work. Applied Sciences. 11(7): 3049.

[26] Alidokht, S.A., Abdollah-zadeh, A., Soleymani, S., Saeid, T. and Assadi, H. 2012. Evaluation of microstructure and wear behavior of friction stir processed cast aluminum alloy. Materials Characterization. 63: 90-97.

[27] Heidarzadeh, A., Kazemi-Choobi, K., Hanifian, H. and Asadi, P. 2014. Microstructural evolution, Advances in Friction-Stir Welding and Processing. Woodhead Publishing, Elsevier.

[28] Marzbanrad, J., Akbari, M., Asadi, P. and Safaee, S. 2014. Characterization of the influence of tool pin profile on microstructural and mechanical properties of friction stir welding Metallurgical and Materials Transactions B. 45:1887–1894.

[29] Shinoda, T. and Kawai, M. 2003. Surface modification by novel friction thermomechanical process of aluminum alloy castings. Surface and Coatings Technology. 169–170: 456-459.

[30] Dolatkhah, A., Golbabaei, P., Besharati Givi, M.K. and Molaiekiya, F. 2012. Investigating effects of process parameters on microstructural and mechanical properties of al5052/sic metal matrix composite fabricated via friction stir processing. Materials & Design. 37: 458-464.

[31] Shafiei-Zarghani, A., Kashani-Bozorg, S.F. and Zarei-Hanzaki, A. 2009. Microstructures and mechanical properties of al/al2o3 surface nano-composite layer produced by friction stir processing. Materials Science and Engineering: A. 500(1–2): 84-91.